Physics of the Dark Universe 47 (2025) 101769

Contents lists available at ScienceDirect

Physics of the Dark Universe

journal homepage: www.elsevier.com/locate/dark

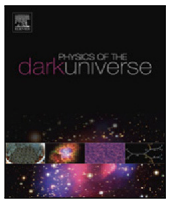

Full length article

Multi-field TDiff theories for cosmology

Diego Tessainer *, Antonio L. Maroto, Prado Martín-Moruno

Departamento de Física Teórica and Instituto de Física de Partículas y del Cosmos (IPARCOS-UCM), Universidad Complutense de Madrid, 28040, Madrid, Spain

ARTICLE INFO

Keywords:
Cosmology
Scalar fields
Shift-symmetry
Transverse diffeomorphisms
Dark energy
Interacting dark sector

ABSTRACT

We consider theories which break the invariance under diffeomorphisms (Diff) down to transverse diffeomorphisms (TDiff) in the matter sector, consisting of multiple scalar fields. In particular, we regard shift-symmetric models with two free TDiff scalar fields in a flat Robertson-Walker spacetime (FLRW) and use the perfect fluid approach to study their dynamics. As a consequence of the symmetry breaking, an effective interaction between the fields is induced from the conservation of the total energy–momentum tensor, without the necessity to introduce any explicit interacting term in the Lagrangian. We study the different single-field domination regimes and analyze the energy exchange between the fields. Thereupon, we introduce an application of these models for the description of interactions in the dark sector, and compare the theoretical predictions of our model to observational data from Type Ia supernovae.

1. Introduction

It is widely known, as observational data indicate, that our Universe currently exhibits an accelerated expansion [1]. Many models explain this as the consequence of a dark energy component dominating the cosmic expansion, taken to be a cosmological constant in the standard model. However, there are other alternatives, such as *quintessence*, involving a canonical scalar field with a dynamical equation of state determined by its potential [2], and *k-essence* [3], which also display dynamical dark energy and can avoid fine-tuning problems, but include non-canonical kinetic terms in the action. Additionally, observational data also indicate that most of the matter composition of our Universe is dark matter [4]. Furthermore, it is nowadays recognized that there exists a tension in the Hubble parameter H_0 measurements [5–7], which could be alleviated by models involving dark sector interactions [8] or phantom models [9], in which the energy density of the dark energy component increases with the expansion. In addition, it has been proven that in order to ease both the H_0 and S_8 cosmological tensions simultaneously by taking into account new physics that is relevant only at late cosmic times, a dark energy component crossing the phantom limit is necessary [10]. On the other hand, as the nature of the dark sector is unknown, possible modifications of gravity at cosmological scales are often considered [11]. Regarding this possibility, multiple modified gravity theories extending upon General Relativity (GR) have been explored [12].

Even if GR provides a very powerful tool for studying gravity and cosmology, theories breaking invariance under diffeomorphisms (Diff) have been recently gaining popularity, with one of the most prominent ones being Unimodular Gravity (UG) [13–15]. In UG, the metric determinant is taken to be a fixed non-dynamical field and the Diff invariance is broken down to transverse diffeomorphisms (TDiff) and Weyl rescalings. UG theories could provide a solution to the problem of vacuum-energy which does not gravitate in this type of theories [16]. Nevertheless, in this work we will focus on theories that are only invariant under TDiff, which have lately started to be studied more deeply. Thus for instance, TDiff models beyond UG have been studied in Refs. [17–20]. The cosmological evolution in TDiff-invariant theories propagating a scalar graviton mode was analyzed in Ref. [19]. On the other hand, TDiff invariant models with broken diffeomorphisms in the matter sector have been analyzed in Refs. [21,22] for single scalar fields. There it is shown that even though on small scales such theories behave as standard Diff models, on super-Hubble scales the behavior can be drastically different, thus opening up a wide range of possibilities for cosmological model building. Thus, in particular, a simple TDiff model for dark matter based on a free scalar field was proposed in Refs. [21,22]. A unified TDiff model for the dark sector has been considered in Ref. [23]. A general classification of single-field TDiff models based on their speed of sound and equation of state was performed in Ref. [24]. TDiff models for single abelian gauge fields can be found in Ref. [25] and their phenomenological implications for cosmic magnetic field evolution in Ref. [26].

In this work we will extend the previous works and consider multi-scalar TDiff invariant models in the matter sector in flat Robertson-Walker (FLRW) spacetimes. We will specifically regard shift-symmetric

* Corresponding author.
E-mail addresses: dtessain@ucm.es (D. Tessainer), maroto@ucm.es (A.L. Maroto), pradomm@ucm.es (P. Martín-Moruno).

https://doi.org/10.1016/j.dark.2024.101769
Received 25 September 2024; Received in revised form 27 November 2024; Accepted 5 December 2024
Available online 12 December 2024

models, which are invariant under shift transformations of the field, i.e., $\phi \to \phi + C$, where C is a constant. Thus, we will only consider the exact kinetic domination regime for each field. The motivation behind this approach lies in the fact that in this way we can avoid fine-tuning problems depending on the specific choice for the potential term in the action. On the other hand, not considering any mass or potential-like terms in the action also results in the Einstein–Hilbert action only receiving higher-order radiative corrections, which also motivates our choice to only break the Diff symmetry in the matter sector.

Unlike the single-field case, the energy–momentum tensor (EMT) conservation will entail an effective interaction between the fields as a consequence of the symmetry breaking even without introducing any interaction terms in the Lagrangian. This fact opens up a wide range of phenomenological implications for multi-field models. Particularly, we will apply this effect to describe an interacting dark sector, comparing its predictions with observational data.

The work is organized as follows. In Section 2 we briefly review the TDiff formalism, focusing on shift-symmetric theories and lay the groundwork for our particular models. Section 3 is devoted to explain the theoretical framework for multi-scalar TDiff models. In Section 4 we perform a numerical analysis for our model, applying it to the dark sector. Results will be compared both with observations and wCDM, and physical predictions for our TDiff model will be obtained. Finally, in Section 5 we will discuss the conclusions.

2. Single-field shift-symmetric TDiff theories

In this section we will briefly recap the main results obtained for shift-symmetric TDiff theories involving one scalar field.

2.1. Transverse diffeomorphisms and matter action

Let us first consider a general infinitesimal coordinate transformation $x^\mu \mapsto x'^\mu = x^\mu + \xi^\mu(x)$ given by the vector field ξ. As it is well known, the variation of metric tensor $g_{\mu\nu}(x)$ will be given by its Lie derivative, i.e.,

$$\delta g_{\mu\nu} = \mathfrak{L}_\xi(g_{\mu\nu}) = -\nabla_\nu \xi_\mu - \nabla_\mu \xi_\nu, \tag{1}$$

and thus it follows that the metric determinant ($g := |\det(g_{\mu\nu})|$) will transform according to

$$\delta g = g g^{\mu\nu}\delta g_{\mu\nu} = -2g\nabla_\mu \xi^\mu. \tag{2}$$

Let us now write down our action. This is

$$S = S_{\rm EH}[g_{\mu\nu}] + S_{\rm mat}[g_{\mu\nu}, \phi], \tag{3}$$

where $S_{\rm mat}$ denotes the matter part of the action involving a single scalar field ϕ. Since we will only break the Diff symmetry in the matter action, the geometrical part will just be the usual Einstein–Hilbert action

$$S_{\rm EH}[g_{\mu\nu}] = -\frac{1}{16\pi G}\int \mathrm{d}^4x\sqrt{g}\,R. \tag{4}$$

On the other hand, the matter part will read

$$S_{\rm mat}[g_{\mu\nu}, \phi] = \int \mathrm{d}^4x\, f(g)\,\mathcal{L}(g_{\mu\nu}(x), \phi(x), \partial_\mu\phi(x)), \tag{5}$$

where $\mathcal{L}$ denotes the corresponding scalar under Diff Lagrangian density and $f(g)$ an arbitrary function of the metric determinant. Recalling (1) and (2) we can compute $\delta_\xi S$, which, after integration by parts and assuming that the fields vanish at infinity, reads [21]

$$\delta_\xi S = \int \mathrm{d}^4x\,\partial_\mu\xi^\mu\,[f(g) - 2g f'(g)]\,\mathcal{L}. \tag{6}$$

Thus, we see that the action is invariant under any infinitesimal coordinate transformation (Diff invariant) only when $f(g) - 2gf'(g) = 0$, i.e. $f(g) \propto \sqrt{g}$. However, the action is also invariant for any form of $f(g)$ if the transformations satisfy $\partial_\mu\xi^\mu = 0$. This corresponds to a smaller subgroup of symmetry, the transverse diffeomorphisms (TDiff).

2.2. Single scalar-field models in the kinetic regime

Let us first consider the matter part of the action with a simple kinetic term [21,22]:

$$S_{\rm mat} = \int \mathrm{d}^4x\,\frac{1}{2}f(g)\,\partial_\mu\phi\partial^\mu\phi, \tag{7}$$

where $f(g)$ is a positive coupling function of the metric determinant. We consider this function to be positive-valued as the wrong sign for the kinetic term is typically related to a ghost instability [27]. The corresponding equation of motion reads

$$\partial_\mu\big(f(g)\partial^\mu\phi\big) = 0\,, \tag{8}$$

and the EMT will be defined as usual:

$$T^{\mu\nu} := -\frac{2}{\sqrt{g}}\frac{\delta S_{\rm mat}}{\delta g_{\mu\nu}}, \tag{9}$$

which in this case reads

$$T_{\mu\nu} = \frac{f(g)}{\sqrt{g}}\left(\partial_\mu\phi\partial_\nu\phi - F(g)\,g_{\mu\nu}\Box\phi\right), \tag{10}$$

where we have defined $F(g) := \mathrm{d}\ln f(g)/\mathrm{d}\ln g$. Since we are not modifying the Einstein–Hilbert action, the Bianchi identities are preserved and thus the local conservation of the EMT will still hold [21,22] under solutions of Einstein equations.

In relation to the background geometry, we will consider a spatially flat FLRW metric. Since we have less gauge freedom than in the Diff case, we will not generally be able to perform a coordinate change that fixes the lapse function to one and we will have more physical degrees of freedom than in the Diff case. Thus, our spacetime can be described by the following line element [28]:

$$ds^2 = b^2(\tau)\,\mathrm{d}\tau^2 - a^2(\tau)\,\mathbf{dx}^2, \tag{11}$$

where $a(\tau)$ and $b(\tau)$ are the independent components that will act as the scale factor and lapse function, respectively; τ denotes the time-coordinate and $\mathbf{dx}^2$ corresponds to the spatial part of the spacetime metric. Both must be computed from Einstein equations.[1]

Let us now apply the perfect fluid approach. It is worth recalling that, when $\partial_\mu\phi$ is a time-like vector, the EMT (10) takes the form [22]

$$T_{\mu\nu} = (\rho + p)\,u_\mu u_\nu - p\,g_{\mu\nu}, \tag{12}$$

where $\rho = T^0{}_0$ denotes the energy density, $p = -T^i{}_j\,\delta^j{}_i/3$ the pressure, and u_μ is the four-velocity of the fluid, a time-like unit vector. Recalling (10) and using (11) we get

$$\rho = \frac{f(g)}{b^2\sqrt{g}}\,[1 - F(g)]\,(\phi')^2, \tag{13}$$

$$p = \frac{f(g)}{b^2\sqrt{g}}\,F(g)\,(\phi')^2, \tag{14}$$

where we have considered a homogeneous field $\phi = \phi(\tau)$. It is straightforward to see from Eqs. (13) and (14) that

$$w_\phi := \frac{p}{\rho} = \frac{F(g)}{1 - F(g)}; \tag{15}$$

which will generally depend on τ and, thus, the equation of state parameter w_ϕ will generally evolve throughout time. One particular case of interest takes place when the coupling function is a power-law, i.e., $f(g) = kg^\alpha$, where k and α are constants. In this case we obtain for w_ϕ the following result:

$$w_\phi = \frac{\alpha}{1 - \alpha} = \text{const}. \tag{16}$$

Notice how this requires $\alpha < 1$ in order for the weak energy condition to be satisfied [22]. In addition, the zeroth component of the EMT conservation equation $\nabla_\nu T^{\mu\nu} = 0$ yields the usual result [21]:

$$\rho' + 3\frac{a'}{a}(\rho + p) = 0. \tag{17}$$

[1] We will use the signature $(+,-,-,-)$ in this work.

On the other hand, the equation for the G^{00} component of the Einstein tensor yields [28]

$$\left(\frac{a'}{a}\right)^2 = \frac{8\pi G}{3}\rho b^2, \tag{18}$$

which is the usual Friedmann equation in time τ. Notice that it recovers its original form under the coordinate transformation $\mathrm{d}t = b(\tau)\,\mathrm{d}\tau$, where t is the cosmological time. We will denote $' = \mathrm{d}/\mathrm{d}\tau$ and $\cdot = \mathrm{d}/\mathrm{d}t$.

Finally, let us write the equation of motion of $\phi(\tau)$ in this space–time (8):

$$\phi''(\tau) + \phi'(\tau)\frac{L'(\tau)}{L(\tau)} = 0, \tag{19}$$

where $L(\tau) \equiv f(g(\tau))/b^2(\tau)$. This equation of motion implies that

$$\phi'(\tau) = \frac{C_\phi}{L(\tau)}, \tag{20}$$

with C_ϕ a constant parameter. Substituting (20) in Eqs. (13) and (14); factoring out $\rho + p$ in Eq. (17) and recalling $g = b^2a^6$, the conservation law (17) reads

$$\frac{\mathrm{d}}{\mathrm{d}\tau}\ln(a^6) = g'(\tau)\frac{\mathrm{d}}{\mathrm{d}g}\left[\ln\left((1-2F(g))\frac{g}{f(g)}\right)\right], \tag{21}$$

which provides the geometrical constraint that allows the conservation law (17) to be satisfied. This is [21]:

$$\frac{g}{f(g)}(1-2F(g)) = C_g a^6, \tag{22}$$

where C_g is a constant. This geometrical constrain on the metric determinant g allows us to obtain the relation between b and a for any given coupling. For instance, if $f(g) \propto g^\alpha$, Eq. (22) implies that

$$b \propto a^{3\alpha/(1-\alpha)}. \tag{23}$$

Notice that only when we take $\alpha = 1/2$ (Diff limit), we recover the standard stiff-fluid behavior $\rho(a) \propto a^{-6}$ of a kinetically dominated scalar field [29,30]. In conclusion, TDiff symmetry allows for a much wider phenomenology for simple kinetically driven scalar fields.

3. Shift-symmetric multi-field TDiff models

In this section we will extend the previous results to the case of two free shift-symmetric TDiff homogeneous scalar fields in the matter action with different coupling functions. Since both fields will be kinetically driven, our action will read

$$S_{\mathrm{mat}} = \int \mathrm{d}^4x \frac{1}{2}\sum_{i=1}^{2}\left(f_i(g)\,\partial_\mu\phi_i\partial^\mu\phi_i\right), \tag{24}$$

where the respective coupling functions $f_i(g)$ are taken to be positive to avoid the explicit introduction of ghosts in our model [27]. Notice that we did not consider an interaction potential between both fields. As we will see, the energy exchange and the rich phenomenology will arise from geometrical constrains coming from the conservation of the total EMT, since the individual EMTs of each field will not be conserved as a consequence of the symmetry breaking. In fact, since our fields are free, the total EMT will simply be the sum of the individual EMTs of each field:

$$\begin{aligned} T_{\mu\nu} &= T^{(1)}_{\mu\nu} + T^{(2)}_{\mu\nu} \\ &= (\rho_1 + p_1)\,u_\mu u_\nu - p_1\,g_{\mu\nu} + (\rho_2 + p_2)\,u_\mu u_\nu - p_2\,g_{\mu\nu} \end{aligned} \tag{25}$$

For homogeneous fields in a Robertson-Walker background both fields share a common velocity u^μ and

$$\rho_i = \frac{f_i(g)}{b^2\sqrt{g}}\left[1 - F_i(g)\right](\phi_i')^2,\ i = 1,2 \tag{26}$$

$$p_i = \frac{f_i(g)}{b^2\sqrt{g}}F_i(g)\,(\phi_i')^2,\ i = 1,2 \tag{27}$$

where very much as in the single-field case, we have defined $F_i(g) := \mathrm{d}\ln f_i(g)/\mathrm{d}\ln g$, so that the corresponding equations of state read

$$w_i := \frac{p_i}{\rho_i} = \frac{F_i(g)}{1 - F_i(g)},\ i = 1,2 \tag{28}$$

The conservation of the total energy–momentum tensor implies

$$\nabla_\mu T^{\mu\nu} = \nabla_\mu T^{(1)\mu\nu} + \nabla_\mu T^{(2)\mu\nu} = 0, \tag{29}$$

which in the Robertson-Walker background reads

$$\rho_1' + 3\frac{a'}{a}(\rho_1 + p_1) + \rho_2' + 3\frac{a'}{a}(\rho_2 + p_2) = 0. \tag{30}$$

Notice that the previous expression does not imply the energy conservation for individual fields, but in general we will have

$$\rho_1' + 3\frac{a'}{a}(\rho_1 + p_1) = Q, \tag{31}$$

$$\rho_2' + 3\frac{a'}{a}(\rho_2 + p_2) = -Q, \tag{32}$$

where Q is commonly referred to as the *interacting kernel* in the literature [31].

On the other hand, the fields equations of motion read

$$\phi_i''(\tau) + \phi_i'(\tau)\frac{L_i'(\tau)}{L_i(\tau)} = 0,\ i = 1,2 \tag{33}$$

with $L_i(\tau) \equiv f_i(g(\tau))/b^2(\tau)$, so that very much as in the single-field case, we can write

$$\phi_i'(\tau) = \frac{C_{\phi_i}}{L_i(\tau)},\ i = 1,2 \tag{34}$$

with C_{ϕ_i} constants.

Substituting these expressions into the respective pressures and energy densities (26) and (27), recalling the conservation Eq. (30) and proceeding analogously to the single-field case, calculations yield the following geometrical constrain:

$$C_{\phi_1}^2\frac{g|2F_1 - 1|}{f_1} + C_{\phi_2}^2\frac{g|2F_2 - 1|}{f_2} = C_g a^6, \tag{35}$$

In the case in which the coupling functions are simple power laws

$$f_i(g) = \lambda_i g^{\alpha_i}, \quad i = 1,2; \tag{36}$$

with λ_i, α_i constants, the conservation Eq. (35) implies

$$C_1 g^{1-\alpha_1}|2\alpha_1 - 1| + C_2 g^{1-\alpha_2}|2\alpha_2 - 1| = C_g a^6; \tag{37}$$

where $C_1 = C_{\phi_1}^2/\lambda_1$ and $C_2 = C_{\phi_2}^2/\lambda_2$. This is a very illuminating result, since as we observe from Eq. (37) it does not require the individual EMT conservation of each field and thus it will involve a geometrical-like interaction between the two components caused by the symmetry breaking. Unlike the single-field case, an explicit solution of this equation cannot be obtained even for simple power-law functions.

Lastly, here we include the expression for the energy density in the power-law coupling case, which will be of valuable use throughout the rest of the work:

$$\rho_i(a,b) = C_i(1-\alpha_i)\frac{b^{1-2\alpha_i}}{a^{6\alpha_i+3}},\ i = 1,2 \tag{38}$$

which is straightforwardly obtained from Eq. (26) using (34). Notice how the effective interactions will be reflected on the particular form of $b(a)$ obtained through the EMT conservation law (37).

3.1. Approximate results: single-field domination

Let us first consider the case in which one of the fields, for example ϕ_1, dominates over the other, ϕ_2. We can thus neglect the contribution of ϕ_2 in (37), so

$$C_1 g^{1-\alpha_1}|2\alpha_1 - 1| \simeq C_g a^6, \tag{39}$$

which can be solved as

$$b \propto a^{3w_1} \tag{40}$$

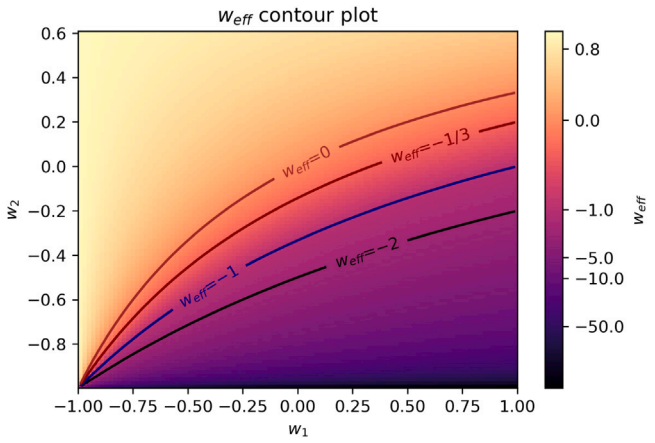

Fig. 1. Effective equation of state parameter w_{eff} of the subdominant field ϕ_2 under ϕ_1 domination in terms of the individual equation of state parameters w_1 and w_2.

where

$$w_1 = \frac{\alpha_1}{1-\alpha_1}, \tag{41}$$

$$w_2 = \frac{\alpha_2}{1-\alpha_2}, \tag{42}$$

as we can see from (28). This is the same geometrical constrain one would obtain if ϕ_1 was the only field. Notice that this is just an approximation that provides the leading order of $b(a)$, but it gives us valuable information concerning the evolution of the energy densities in the different domination regimes. Recalling (38) and using (40) yields

$$\rho_1(a) \propto a^{-3(1+w_1)} \quad \text{and} \quad \rho_2(a) \propto a^{-3(1+w_{\text{eff}})}, \tag{43}$$

and thus ϕ_1 decays as expected from its equation of state, but the subdominant field ϕ_2 will exhibit a decay as if it were a perfect fluid with constant equation of state parameter $w_{\text{eff}} \neq w_2$, where

$$w_{\text{eff}} = \frac{2w_2 - w_1 + w_1 w_2}{1+w_2}. \tag{44}$$

It is worth noting that the individual equation of state parameters w_i will then depict the asymptotic decay behavior of each component when it is dominant. Fig. 1 summarizes the wide range of phenomenological possibilities for the subdominant component.

This result happens to be physically illuminating with regards to cosmological contexts. As we can see above, the induced interactions between perfect TDiff fluids with different equation of state parameters allow for a wide range of possible evolutions for the subdominant component. In particular, all of the possible dark energy behaviors are plausible for the subdominant field, including phantom dark energy [32] ($w_{\text{eff}} < -1$, where its energy density increases over time) and quintessence. We emphasize that these behaviors can be obtained without the addition of non-canonical kinetic terms [3], they are a result of breaking the Diff symmetry down to TDiff. Interestingly, although $w_i < -1$ is not allowed for each individual field, in accordance to the weak energy condition [22], the dominance regimes allow for subdominant phantom behavior without violating the energy conditions. As a result, this provides a vast range of possibilities to describe an interacting dark matter-dark energy sector ($w_1 = 0$, $w_2 < -1/3$) with an evolving dark energy decay given by a function $w_{\text{eff}}(a)$ stemming from the broken Diff invariance, exhibiting phantom decay at early times during the matter epoch. This will allow for phantom-crossing, as it will later be discussed.

3.2. Energy exchange

We will now analyze the exchange of energy between the fields induced by the effective interaction, and its evolution through the several field domination regimes by studying the interacting kernel Q. Let us consider two kinetically-driven scalar fields ϕ_1 and ϕ_2, with constant equation of state parameters w_1 and w_2, respectively. Let us also assume that ϕ_1 dominates over ϕ_2. Using (38) on Eq. (32) and recalling (44) we obtain the following expression

$$Q = 3C_2(1-\alpha_2)\frac{a'}{a}a^{-3(1+w_{\text{eff}})}(w_{\text{eff}} - w_2). \tag{45}$$

which can be rewritten as

$$Q = 3\rho_2 \mathcal{H}\frac{(w_2 - w_1)(1-w_2)}{1+w_2}. \tag{46}$$

where $\mathcal{H} = a'/a$ denotes the Hubble parameter in time coordinate τ. It is worth mentioning that, according to (46), we will not be able to recover the ΛCDM limit in this model, as when one of the fields starts to approximately behave like a cosmological constant in its asymptotic domination regime ($w_i \to -1$), Q will diverge and both TDiff components will thus be strongly coupled. This behavior is linked to the shift-symmetric nature of the fields, which do not have potential terms.

Let us now study the sign of Q during the single-field domination regimes. Firstly, we observe from (46) that when ϕ_1 dominates, Q has two zeros, those being at $w_{\text{eff}} = w_2$, i.e., $w_2 = w_1$ and $w_2 = 1$. On the other hand, the analysis in the ϕ_2 domination regime is fully akin to the previous one, but we have to perform the change $w_1 \mapsto w_2$ and change the sign of Q (remember we defined Q with respect to the conservation law for ϕ_1). We show in Fig. 2 the sign of the interaction kernel in both cases (ϕ_1 and ϕ_2 domination).

In light of this analysis, we distinguish three scenarios. In the first case, in which both equation of state parameters are smaller than one ($w_1, w_2 < 1$), the sign of Q does not change between both domination regimes and thus the direction of the energy exchange will not be altered over time. More clearly, if we assume $w_1 > w_2$ we see from Fig. 2 that when ϕ_1 dominates $Q < 0$ and ϕ_1 loses energy in favor of ϕ_2, with the same happening as well when ϕ_2 is dominant. The same reasoning can be applied to the case in which $w_1 < w_2$ (although in this case $Q > 0$), allowing us to conclude that in this case it is the field with the greater equation of state parameter who always loses energy.

Secondly, we also have the case in which both fields are beyond stiff fluids ($w_1, w_2 > 1$). We can immediately check (see Fig. 2), similarly to how we proceeded in the previous case, that the direction of the energy exchange will not change during the interaction and it will always be the field with the larger equation of state parameter which gains energy from the other component.

Lastly, there is the case in which one of the fields is beyond a stiff fluid and the other is not ($w_1 > 1$, $w_2 < 1$ and vice versa). As opposed to the previous scenarios, we see from Fig. 2 that the direction of the energy flux changes between both domination regimes. For instance, if $w_1 > 1$ and $w_2 < 1$, Q will be smaller than zero under ϕ_1 domination and thus ϕ_2 will be gaining energy from ϕ_1. However, when ϕ_2 is dominant, since $w_1 > 1$ we can see that $Q > 0$ and thus it is ϕ_1 which gains energy from ϕ_2 now (the analysis is analogous if $w_1 < 1$, $w_2 > 1$).

Regarding the potential applications for the description of the dark sector, notice that in (44) $w_{\text{eff}} = -1/3$ when $w_2 = (-1+3w_1)/(7+3w_1) \equiv \mathcal{A} < w_1$. This separates the region of w_2 values in which the subdominant field, taken to be ϕ_2 for this example, starts decaying as dark energy. Similarly, $w_{\text{eff}} = -1$ occurs at $w_2 = (-1+w_1)/(3+w_1) \equiv \mathcal{B}$ and it corresponds to the phantom behavior boundary for ϕ_2. Hence, if $w_1 < 1$ we can see that if $w_2 \in (-1, \mathcal{B})$ the subdominant component will exhibit phantom dark energy behavior and the dominant field will lose energy in favor of this; and if $w_2 \in (\mathcal{B}, \mathcal{A})$ it will also gain energy from the dominant component ϕ_1, but not enough to display phantom nature.

More specifically, if we consider a dark sector model consisting of dark matter (DM) with $w_1 = 0$ and dark energy (DE), with $w_2 < -1/3$, we can observe from (44) that DE will always be phantom during the matter domination epoch due to the energy flux from DM ($Q < 0$). The

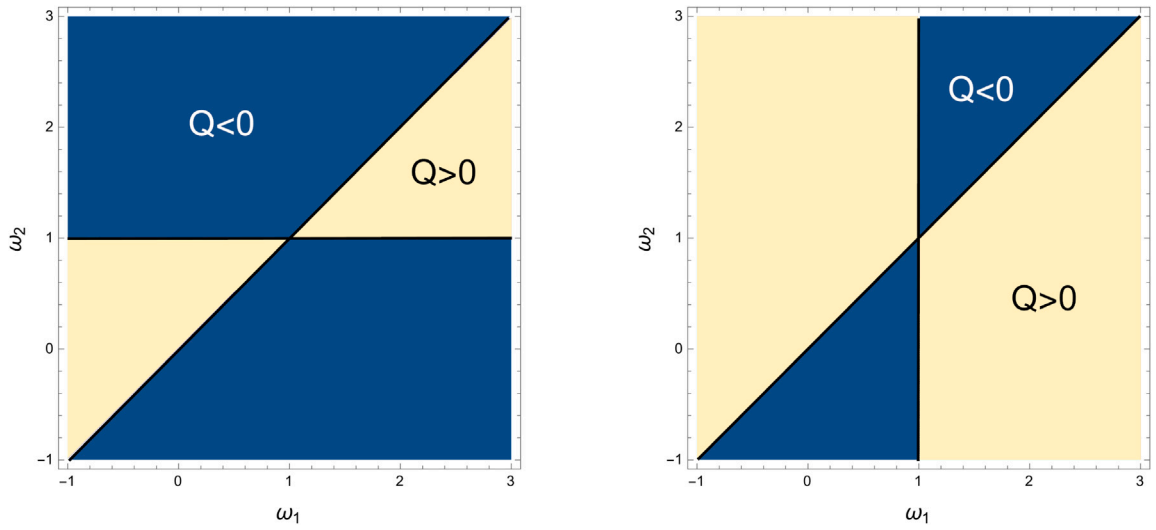

Fig. 2. Sign of the interaction kernel Q when the ϕ_1 fluid dominates (left) and for ϕ_2 domination (right).

energy exchange will occur in the same direction when DE dominates, although it will now not be enough to keep the phantom behavior, and the DE decay will gradually transition to resemble its asymptotic value for the equation of state parameter w_2. On the other hand, DM will slowly start to exhibit a different decay than the typical a^{-3} as DE becomes more dominant.

Lastly, before we go on with our analysis let us briefly comment about the existence of tracking solutions in this model. Recalling (43) we see that the condition that must be satisfied in order for both fields to exhibit the same decay would be

$$-3(1+w_1) = \frac{3w_1 - 9w_2 - 3w_1w_2 - 3}{1+w_2}, \tag{47}$$

which cannot be accomplished unless we are in the trivial case in which both components are indeed the same, i.e., $w_1 = w_2$, and there would be no interaction. Thus, there will not be tracking solutions in this particular TDiff model.

3.3. Analytical model

Solving the general constrain (37) is not a simple task, and it usually requires numerical treatment. However, there is a particular dark sector model for which Eq. (37) can be analytically solved, consisting of DM with $w_1 = 0$ ($\alpha_1 = 0$) and DE with $w_2 = -1/2$ ($\alpha_2 = -1$). Despite not being the best fitting model, as we will later see, being analytical provides us with a wide insight to further understand the physics behind shift-symmetric multi-field TDiff models. The constrain (37) then reads

$$C_1 g + 3C_2 g^2 = C_g a^6, \tag{48}$$

which is quadratic in g and can be easily solved as

$$g = -\frac{C_1}{6C_2} + \frac{\sqrt{C_1^2 + 12C_2C_g a^6}}{6C_2}, \tag{49}$$

where we have taken into account that $C_i = C_{\phi_i}^2/\lambda_i$ should be positive to avoid ghosts instabilities, so that only the positive-root solution of Eq. (48) is physically sensible. This solution allows us to explicitly obtain the relation $b(a)$:

$$b(a) = \sqrt{\frac{C_1}{6C_2}}\left[a^{-6}\left(\sqrt{1 + \frac{12C_2C_g}{C_1^2}a^6} - 1\right)\right]^{1/2}, \tag{50}$$

valid for all values of a. As we will later see, the remote past $a \ll 1$ will correspond to the matter era, and in the distant future $a \gg 1$ DE will be dominant, as expected.

For $a \ll 1$, expanding (50) in powers of a yields

$$b(a)\Big|_{a\ll 1} \simeq \sqrt{C_g}C_1\left(1 - \frac{3}{2}\frac{C_2C_g}{C_1^2}a^6\right), \tag{51}$$

from which we can obtain the respective energy densities:

$$\rho_1(a) \simeq \sqrt{C_1C_g}\left(a^{-3} - \frac{3C_2C_g}{2C_1^2}a^3\right), \tag{52}$$

$$\rho_2(a) \simeq 2\left(\frac{C_g}{C_1}\right)^{3/2} C_2 a^3. \tag{53}$$

Notice how the DM (ρ_1) decay is governed by the a^{-3} term, which corresponds to the expected behavior according to $w_1 = 0$. Consequently, DM is dominant at early times. Besides, DE (ρ_2) evolves with a^3, exhibiting the phantom nature we previously discussed (in particular, $w_{\text{eff}} = -2$) as a result of it gaining energy from DM. This can be illustrated writing the conservation equations for each component in terms of the energy density of the other, which read:

$$\rho_1' + 3\frac{a'}{a}\rho_1 \simeq -\frac{9}{2}\mathcal{H}\rho_2, \tag{54}$$

$$\rho_2' + 3\frac{a'}{a}(\rho_2 + p_2) \simeq +9C_g^2\frac{C_2}{C_1}\mathcal{H}\frac{1}{\rho_1}; \tag{55}$$

where the phantom nature is exposed in (55) as a result of ρ_1 appearing in the denominator.

On the other hand, for $a \gg 1$, expanding (50) yields

$$b(a)\Big|_{a\gg 1} \simeq \sqrt{\frac{C_1}{6C_2}}\left(\sqrt{A}a^{-3/2} - \frac{1}{\sqrt{2A}}a^{-9/2}\right), \tag{56}$$

with $A \equiv \sqrt{12C_2C_g/C_1^2}$. The energy densities thus read

$$\rho_1(a) \simeq \frac{C_1^{3/2}}{\sqrt{6C_2}}\left(\sqrt{A}a^{-9/2} - \frac{1}{2\sqrt{A}}a^{-15/2}\right), \tag{57}$$

$$\rho_2(a) \simeq \frac{C_1^{3/2}}{6^{3/2}C_2^{1/2}}(-3a^{-9/2}\sqrt{A} + 2a^{-3/2}A^{3/2}). \tag{58}$$

The leading order for large values of a in ρ_2 indicates that now our DE will decay as expected from its equation of state ($w_2 = -1/2$), and DM decays faster than a^{-3}. This implies that at later times it is DE who becomes dominant, and from the reasoning of the previous subsection, we can see that DM is still giving energy to DE, but not enough to keep the phantom behavior as DM starts becoming subdominant. One could write analogous expressions to (54) and (55), but they are not as physically enlightening due to the lack of phantom nature under dark energy domination.

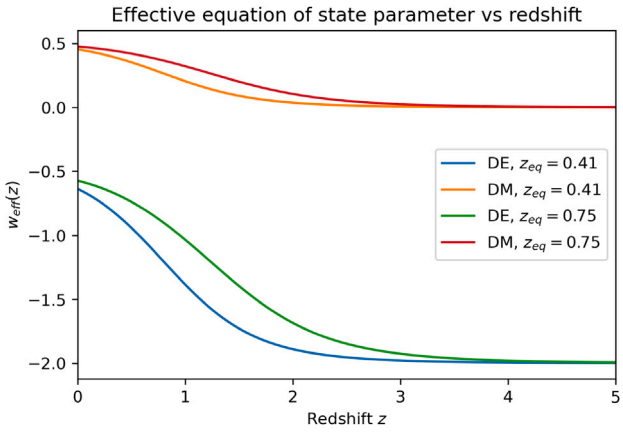

Fig. 3. $w_{\rm eff}(z)$ for DM and DE for various $z_{\rm eq}$. Dark energy transitions from being phantom during the matter era to decaying as usual dark energy with equation of state parameter w_2, with there being phantom crossing at recent times. Dark matter starts to decay faster than expected from $w_1 = 0$ as dark energy starts dominating.

We will now write the exact expressions for both energy densities in order to discuss the whole evolution. From the previous analysis we know that both energy densities become equal at a certain time: $a = a_{\rm eq}$, $\rho_i = \rho_{\rm eq}$. We can thus write ρ_1 and ρ_2 substituting (50) in (38) and equating them. We obtain

$$C_1 = \frac{5}{2}\rho_{\rm eq}^2 a_{\rm eq}^6 C_g^{-1} \quad , \quad C_2 = \frac{125}{16}\rho_{\rm eq}^4 a_{\rm eq}^6 \frac{1}{C_g^3}; \tag{59}$$

which allow us to write down the energy densities in terms of these parameters, which are easier to physically interpret than the integration constants C_i. Thus, we have:

$$\rho_1(z) = \frac{1}{\sqrt{3}}\rho_{\rm eq}\left(\frac{1+z}{1+z_{\rm eq}}\right)^6 \Theta^{1/2}(z), \tag{60}$$

$$\rho_2(z) = \frac{1}{\sqrt{27}}\rho_{\rm eq}\left(\frac{1+z}{1+z_{\rm eq}}\right)^6 \Theta^{3/2}(z); \tag{61}$$

where we defined $\Theta(z) \equiv \sqrt{1 + 15[(1+z_{\rm eq})/(1+z)]^6} - 1$, and where $z = 1/a - 1$ denotes the redshift.

We will now obtain some physical results and compare this model to ΛCDM before analyzing the general case. Firstly, recalling (38) and the conservation law (17), we can parameterize the decay of each component with a function $w_{\rm eff,i}(z)$ which satisfies the individual conservation law

$$\rho'_i + 3\frac{a'}{a}[1 + w_{\rm eff,i}(z)]\,\rho_i = 0; \tag{62}$$

which yields the following result when recalling (38):

$$w_{\rm eff,i}(z) = -\frac{1}{3}\left[-\frac{1+z}{b(z)}(1-2\alpha_i)\frac{{\rm d}b}{{\rm d}z} - 6\alpha_i - 3\right] - 1, \tag{63}$$

where α_i denote the exponents of the coupling functions of each component. This recovers the previously studied constant results when considering the respective field domination regimes. The functions $w_{\rm eff,i}(z)$ can easily be simplified for the analytical case since we know $b(z)$ explicitly.

Using the exact expression for $b(z)$ (50) yields the result in Fig. 3, for two different values of the free parameter $z_{\rm eq}$. Notice how in reality we only have $z_{\rm eq}$ as our free parameter, since the cosmic sum rule $(\rho_1 + \rho_2)\big|_{t=t_0} = (1 - \Omega_{\rm B})\rho_{\rm c}$ must be satisfied and, thus, it enforces an extra relation between the parameters that allows to remove the dependence on $\rho_{\rm eq}$. As a reminder, $\Omega_{\rm B}$ depicts the baryonic matter component of the universe, $\rho_{\rm c}$ is the critical density and we are ignoring the radiation component at late times. It is worth noting that in this work we assumed that only the dark sector breaks the Diff invariance, hence we will treat baryons as ordinary Diff matter. As we can see from Fig. 3, the DE decay behavior starts being phantom-like at early times, as expected, and then evolves in time until it reaches the asymptotic value reflected in the equation of state $w_2 > -1$ in the future, with there being phantom-crossing near the present. The parameter $z_{\rm eq}$ only changes slightly the behavior in the intermediate regimes, without altering the main physical behavior. On the other hand, DM will exhibit its usual a^{-3} decay at early times but it will decay faster when DE starts to dominate. In light of this we can see that TDiff models can provide a very rich phenomenology involving different time evolutions for the dark sector. This could lead to new models for interactions in the dark sector without the introduction of non-canonical terms or ghost instabilities in the action.

Lastly, we will analyze this model from the perspective of the density parameters to further understand shift-symmetric TDiff dark sector models. We will denote the density parameters for DM and DE, respectively, as $\Omega_{\rm DMT}$ and $\Omega_{\rm DET}$. We will also use the standard notation for the ΛCDM parameters: $\Omega_{\rm M} = \Omega_{\rm DM} + \Omega_{\rm B}$ for matter and Ω_Λ for the cosmological constant. Recalling the Friedmann Eq. (18) and using cosmological time ${\rm d}t = b(\tau){\rm d}\tau$ yields

$$H^2 = \frac{8\pi G}{3}(\rho_{\rm B} + \rho_1 + \rho_2). \tag{64}$$

Multiplying and dividing this expression by the Hubble parameter at $t = t_0$ (today) H_0^2, and recalling that $\rho_{\rm c} = 8\pi G/(3H_0^2)$ it is straightforward to obtain the respective abundances in terms of the redshift, $\Omega_i(z) = 8\pi G\rho_i(z)/[3H^2(z)]$:

$$\Omega_{\rm DMT}(z) = \frac{1}{\sqrt{3}}\frac{\rho_{\rm eq}}{\rho_{\rm c}}\left(\frac{1+z}{1+z_{\rm eq}}\right)^6 \frac{\Theta^{1/2}(z)}{E^2(z)}, \tag{65}$$

$$\Omega_{\rm DET}(z) = \frac{1}{3\sqrt{3}}\frac{\rho_{\rm eq}}{\rho_{\rm c}}\left(\frac{1+z}{1+z_{\rm eq}}\right)^6 \frac{\Theta^{3/2}(z)}{E^2(z)}, \tag{66}$$

where we defined

$$E^2(z) \equiv \Omega_{\rm B}(1+z)^3 + \frac{\rho_{\rm eq}}{\sqrt{3}\rho_{\rm c}}\left(\frac{1+z}{1+z_{\rm eq}}\right)^6 \Theta^{1/2}(z)\left[1 + \frac{\Theta(z)}{3}\right]. \tag{67}$$

This allows us to obtain the time evolution for each density parameter. This will obviously depend on the specific value of $z_{\rm eq}$, but the general behavior will be similar. For the sake of simplicity, we included the case $z_{\rm eq} = 1.1$ in Fig. 4 to show qualitative results. This results in a higher DE abundance and a lower DM one at $t = t_0$ than those from ΛCDM, which can be interpreted as a consequence of the phantom era during the DM domination regime. As we previously discussed, DM transfers part of its energy to DE, which translates into its phantom behavior and thus contributes to obtaining higher values of $\Omega_{\rm DET}$. It is worth mentioning, however, that we shall not directly compare these parameters to those from ΛCDM, as $\Omega_{\rm DMT}$ and $\Omega_{\rm DET}$ may not be regarded as *true* DM and DE density parameters, since, as opposed to ΛCDM, this model presents an interacting dark sector and thus there may be contributions from both components to each parameter.

4. A TDiff model for dark sector interactions

We will now consider a more general case with $w_1 = 0$, which could play the role of DM; and arbitrary $w_2 < -1/3$, which could play the role of DE. We will then contrast the predictions of this simple model to observations to get a glimpse on the viability of shift-symmetric TDiff models for describing the dark sector. Recalling the geometrical constrain (37) arisen from the conservation of the EMT, using $\alpha_1 = 0$ and dividing by C_2 yields

$$\lambda(1-\alpha_2)g + g^{1-\alpha_2}|2\alpha_2 - 1| = a^6\left(\lambda(1-\alpha_2) + |2\alpha_2 - 1|\right). \tag{68}$$

where we have used

$$\frac{\rho_1(t_0)}{\rho_2(t_0)} = \frac{C_1}{C_2}(1-\alpha_2)^{-1} = \frac{\Omega_{\rm DMT}}{\Omega_{\rm DET}} \equiv \lambda. \tag{69}$$

and normalized[2] $a(t_0) = 1$, and also $g(t_0) = 1$, which leads to $b(t_0) = 1$. Therefore, we only have two free parameters, those being the exponent

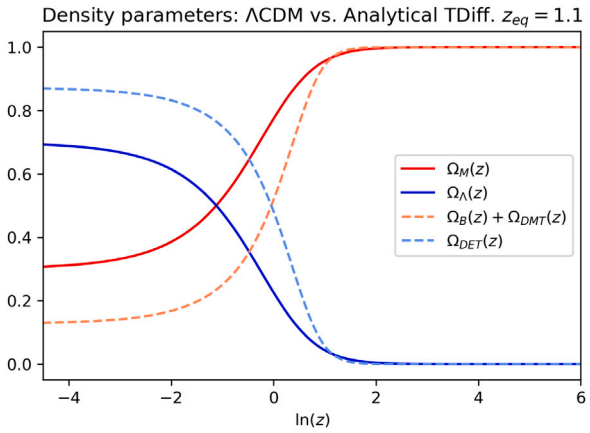

Fig. 4. Evolution of the density parameters: ΛCDM (continuous lines) vs analytical TDiff case (dashed lines), for $z_{\rm eq} = 1.10$. In shift-symmetric TDiff models dark energy would be more dominant as a consequence of it being phantom at early times, gaining energy from dark matter.

of the power-law coupling function of the DE component, α_2, and λ. However, we will use another physical parameter instead of λ in order to obtain a more direct analysis and an easier comparison to observations. In fact, recalling Friedman Eq. (64) in cosmological time, using (38) and noting that $(\rho_1+\rho_2)\big|_{t_0} = (1-\Omega_{\rm B})\rho_{\rm c}$ as a consequence of the cosmic sum rule yields the following expression for $H^2(z)$:

$$H^2(z) = H_0^2\left[\Omega_{\rm B}(1+z)^3 + (1-\Omega_{\rm B})\left(1+\frac{1}{\lambda}\right)^{-1} b(z)(1+z)^3 + (1-\Omega_{\rm B})\frac{1}{\lambda}\left(1+\frac{1}{\lambda}\right)^{-1} b(z)^{1-2\alpha_2}(1+z)^{6\alpha_2+3}\right], \tag{70}$$

where we neglected radiation, as the purpose of this model is to study the DM and DE domination epochs. Otherwise, we should have included the corresponding $\Omega_{\rm R}(1+z)^4$ contribution from radiation, where we are assuming it is a Diff component.[3] Notice that at early times, when the ϕ_1 fluid dominates over ϕ_2, we can neglect the last term in (70). In addition, $b(a) \propto a^{3w_1}$ takes a constant value at early times $b(z) \simeq b_{early}$ since $w_1 = 0$. This allows us to define the following effective density parameter for total matter at high redshift

$$\Omega_{\rm M}^{\rm eff} \equiv \Omega_{\rm B} + (1-\Omega_{\rm B})\left(1+\frac{1}{\lambda}\right)^{-1} b_{\rm early}. \tag{71}$$

We will use this parameter $\Omega_{\rm M}^{\rm eff}$ instead of λ, since both are trivially related through (71). Acknowledge that $b_{\rm early}$ can be directly computed from the conservation Eq. (68) taking into consideration that DM dominates at this time and radiation does not contribute to the geometrical constrain, since we are treating it as a Diff component and thus its EMT is automatically conserved. Thus, using (69) we obtain

$$b_{\rm early} = \sqrt{\frac{\lambda(1-\alpha_2)+|2\alpha_2-1|}{\lambda(1-\alpha_2)}}. \tag{72}$$

If we express H_0^{-1} as $2997.9h^{-1}$ Mpc, with h being the reduced Hubble constant, this will allow us to fit our parameters $(w_2, \Omega_{\rm M}^{\rm eff})$ to observations and obtain physical predictions for this model. Notice that we are using w_2 instead of α_2 as the model parameter since the are trivially related by (42). We will consider the baryon density parameter obtained from the abundance of light elements $\Omega_{\rm B}h^2 = 0.02240 \pm 0.00069$ [33], as it is independent of the particular choice for the cosmological model, and we will marginalize the absolute magnitude M, which is equivalent to marginalize H_0 since they are degenerated, as we will later explain (for the supernovae analysis) [34]. In particular, we developed a code in *Python* that solves the conservation law (68) for any given pair of these two parameters. Hence, we can obtain $b(z)$ and $H(z)$ through (70). We will then regard different data sets (namely Union2 supernovae and CMB) and perform a preliminary numerical likelihood analysis in order to study the validity of the model. We will then present the structure of the analysis in the following subsections.

4.1. Union2 supernovae data set

We will first consider the Union2-database observational data coming from type Ia Supernovae [35,36] consisting of 557 data for $0.015 < z < 1.030$ and compare them to the theoretical distance moduli $\mu(z)$ predictions of our model. We will study the agreement between theory and observations using the χ^2 statistical estimator [37]:

$$\chi^2_{\rm SNIa} = \sum_i \frac{(\mu^{\rm obs}(z_i) - \mu^{\rm th}(z_i))^2}{E_i^2}, \tag{73}$$

where E_i denotes the error in the μ_i measurement at redshift z_i and the theoretical distance modulus is given by

$$\mu^{\rm th}(z) = 5\log_{10}\left(\frac{d_{\rm L}(z)}{1\ {\rm Mpc}}\right) + M = \hat{\mu}(z) + M, \tag{74}$$

with $d_{\rm L}(z)$ the luminosity distance computed from

$$d_{\rm L}(z) = (1+z)\int_0^z \frac{{\rm d}z}{H(z)}, \tag{75}$$

for flat spatial sections and M being the absolute magnitude, which we marginalized the following way:

$$M = \sum_i \left(\frac{1}{\sigma}\frac{\mu^{\rm obs}(z_i) - \hat{\mu}(z_i)}{E_i^2}\right). \tag{76}$$

with $\sigma = \sum_i E_i^{-2}$. Notice that this is equivalent to marginalizing H_0, as it is degenerated with M, according to (74). Numerical integration will allow us to perform the analysis in the subsequent sections.

4.2. CMB data set

We will also consider the CMB data to study the observational viability of our model. For this purpose, we will be using the two CMB distance priors R (the shift parameter) and ℓ_a (the acoustic length) [23,38] instead of the Planck 2018 full likelihood, as our model behaves the same way as ΛCDM at early times and these parameters allow us to easily assemble all the relevant information. The respective values measured for these parameters for the Planck 2018 TT,TE,TE+lowE+ lensing data [34] are the following [23]:

$$R = 1.7497 \pm 0.0041, \tag{77}$$

$$\ell_a = 301.529 \pm 0.083, \tag{78}$$

with the covariance matrix given by

$$\mathbf{Cov} = \begin{pmatrix} 6.889\cdot 10^{-3} & 1.2090859\cdot 10^{-4} \\ 1.2090859\cdot 10^{-4} & 1.681\cdot 10^{-5} \end{pmatrix}, \tag{79}$$

which was obtained using the respective correlation matrix presented in [23].

On the other hand, the theoretical expressions used to compute the distance priors read

$$R = \sqrt{\Omega_M^{\rm eff} H_0^2}(1+z_*)d_{\rm A}(z_*), \tag{80}$$

$$\ell_a = \pi(1+z_*)\frac{d_{\rm A}(z_*)}{r_{\rm s}}, \tag{81}$$

[2] Notice how we can fix the second condition $g(t_0) = 1$ as well, since performing this change will be reflected in the action (24) as a global constant C, $\tilde{S}_{\rm mat} = CS_{\rm mat}$; and therefore both actions will be physically equivalent under a redefinition of the fields embodying this change: $\phi_i \mapsto \tilde{\phi}_i = \sqrt{C}\phi_i$.

[3] Hence, its EMT is automatically conserved under solutions of Einstein equations and at early times during the radiation era the model behaves the same way as ΛCDM, as the TDiff components are negligible at such time. Thus, the bounds imposed by BBN are not modified in this model.

Table 1
Two-parameter fit (SNIa): TDiff vs wCDM. Both models show similar agreement with observations. The 1-σ intervals for each parameter have also been included.

SNIa	Best fit	$\chi^2_{\min}$
TDiff	$w_2 = -0.813^{+0.102}_{-0.060}$, $\Omega_M^{\text{eff}} = 0.387^{+0.056}_{-0.078}$	542.16
wCDM	$w = -1.142^{+0.145}_{-0.184}$, $\Omega_M = 0.346^{+0.082}_{-0.083}$	542.64

where $d_A(z)$ denotes the angular distance

$$d_A(z) = \frac{1}{1+z}\int_0^z \frac{dz'}{H(z')}, \tag{82}$$

and r_s denotes the radius of the sound horizon

$$r_s = r(z_*) = \int_{z_*}^{\infty} dz' \frac{c_s(z')}{H(z')}, \tag{83}$$

where $c_s(z)$ is the speed of sound in the photon-baryon fluid. The quantity z_* present in the formulas above depicts the decoupling redshift, whose value is obtained through the fitting expressions in [39]:

$$z_* = 1048(1 + 0.00124\,\omega_B^{-0.738})(1 + g_1\omega_M^{g_2}), \tag{84}$$

$$g_1 = \frac{0.0783\omega_B^{-0.238}}{1 + 39.5\omega_B^{0.763}}, \tag{85}$$

$$g_2 = \frac{0.560}{1 + 21.1\omega_B^{1.81}}. \tag{86}$$

It is worth mentioning that ω_B and ω_M denote the respective reduced baryonic and matter density parameters, i.e., $\omega_B = \Omega_B h^2$ and $\omega_M = \Omega_M^{\text{eff}} h^2$, where we are using Ω_M^{eff} as all of the previous expressions are meant to be evaluated at high redshift, where Ω_M^{eff} is a constant in light of (71) and acts as the usual matter abundance. Similarly, we also must take the radiation term into account in the Hubble rate, that is $\Omega_R(1+z)^4$, when performing this calculations.

Finally, we will also study the accordance between our model and these distance prior data using the χ^2 estimator:

$$\chi^2_{\text{CMB}} = \boldsymbol{\Delta}^T \cdot \mathbf{Cov}^{-1} \cdot \boldsymbol{\Delta}, \tag{87}$$

where $\boldsymbol{\Delta}$ depicts the vector consisting of the differences between the distance prior data and their theoretical values, which depend on the parameters of our TDiff model We will lastly consider the full χ^2 combined function:

$$\chi^2 = \chi^2_{\text{SNIa}} + \chi^2_{\text{CMB}}. \tag{88}$$

4.3. Two-parameter fit

We will now analyze our TDiff model to conclude if the actual best TDiff fit is compatible with type Ia supernovae observations and CMB data. On the grounds of this, for the type Ia supernova fit we considered a grid of values of $w_2 \in (-0.993, -0.50)$ and $\Omega_M^{\text{eff}} \in (0.10, 0.50)$ and computed χ^2_{SNIa} numerically from (73) for the grid marginalizing M (or, equivalently, H_0, as they are degenerated). For the CMB fit we also marginalized H_0, but in a numerical way after having computed the full likelihood grid, as we cannot proceed analytically like we did in (76). We thus considered a parameter grid consisting of values of $w_2 \in (-0.80, -0.42)$, $\Omega_M^{\text{eff}} \in (0.23, 0.41)$ and $h \in (0.59, 0.77)$ and computed χ^2_{CMB} for each case using the distance priors and (87). We then marginalized the Hubble constant and obtained the two-parameter CMB likelihood that we will use to compare both data analyses. In the following analysis we will also include the direct wCDM analogue of this two-parameter fit, in which both Ω_M and w are fitted (using values for w in $(-1.75, -0.45)$ and Ω_M in $(0.05, 0.60)$), in order to compare both models. Numerical analysis thus yields the results in Tables 1–3.

These results indicate that both TDiff and wCDM fit well with the observational data, with the difference between the joint fits for both models being lower than 1-σ (although wCDM presents a slightly better goodness of the fit). Therefore, we will focus on the TDiff case from now on and present the contour plot for both parameters up to the 3-σ region in Fig. 5. The results obtained indicate that TDiff models provide good compatibility when it comes to type Ia supernovae and CMB observations. It is also worth mentioning that the marginalized distributions for our parameters in the CMB fit are not gaussian and exhibit abrupt decays at the extremes, which can be a consequence of a strong correlation and degeneracy between our parameters (see Fig. 5). Lastly, it is worth recalling that this is an exploratory analysis that enables us to check the observational viability of the model and get some constraints in relation with the cosmological parameters. We are also using an approximate CMB likelihood, and thus the full likelihood using other observational sets and all of the observables should be considered in the future.

The respective 1-σ intervals for each of the parameters were obtained by marginalizing the joint likelihood

$$\mathcal{L}(w_2, \Omega_M^{\text{eff}}) = \mathcal{N} e^{-\chi^2_s/2}, \tag{89}$$

Table 2
Two-parameter fit: TDiff vs wCDM (CMB). Both models show agreement with observations. The 1-σ intervals for each parameter have also been included. The - in the χ^2 column indicates that χ^2 is zero for the best fit, as expected since we are fitting two parameters using data for two distance priors. The 68% regions are very asymmetric as a consequence of the non-gaussianity of the probability distributions.

CMB	Best fit	$\chi^2_{\min}$
TDiff	$w_2 = -0.722^{+0.191}_{-0.058}$, $\Omega_M^{\text{eff}} = 0.263^{+0.077}_{-0.016}$	–
wCDM	$w = -1.278^{+0.378}_{-0.042}$, $\Omega_M = 0.236^{+0.097}_{-0.002}$	–

Table 3
Two-parameter fit: TDiff vs wCDM (SNIa+CMB). Both models are in good agreement with observations. The 1-σ intervals for each parameter have also been included. There is a difference of less than 1-σ between both models.

SNIa+CMB	Best fit	$\chi^2_{\min}$
TDiff	$w_2 = -0.703^{+0.026}_{-0.026}$, $\Omega_M^{\text{eff}} = 0.273^{+0.010}_{-0.010}$	557.97
wCDM	$w = -1.092^{+0.034}_{-0.034}$, $\Omega_M = 0.292^{+0.010}_{-0.010}$	556.63

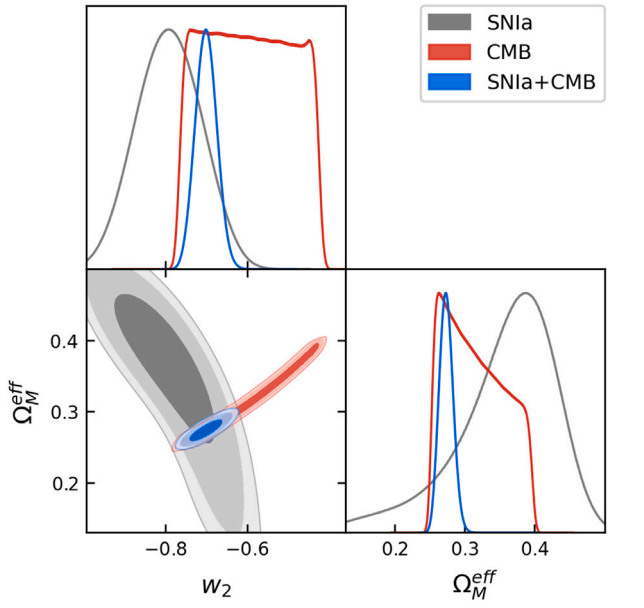

Fig. 5. Two-parameter fit: contour plot for χ^2 up to the 3-σ region using Union2 and CMB data. The 1-σ region for the SNIa and CMB are compatible with each other. Notice that the 68% contour region differs a bit from the marginalized 1-σ intervals, which is a consequence of the non-gaussianity of the distributions.

which can be done for each variable by performing the integration with respect to the other. This yields:

$$\mathcal{L}^{\rm m}(w_2) = \mathcal{N}_1 \int \mathrm{e}^{-\chi_s^2/2}\mathrm{d}\Omega_{\rm M}^{\rm eff}, \quad \mathcal{L}^{\rm m}(\Omega_{\rm M}^{\rm eff}) = \mathcal{N}_2 \int \mathrm{e}^{-\chi_s^2/2}\mathrm{d}w_2; \tag{90}$$

where $\mathcal{N}_1$ and $\mathcal{N}_2$ are normalization constants (the way of proceeding for the wCDM case is fully analogous). The maximization of these marginalized likelihood distributions $\mathcal{L}^{\rm m}$ allowed us to obtain the 1-σ regions for both of the parameters, which has been done making use of the GetDist package for Python.[4] It is worth mentioning that we can estimate the tension between the SNIa and CMB results for w_2 and $\Omega_{\rm M}^{\rm eff}$ using the following expressions:

$$\tau_1 = \frac{\left|w_2^{\rm SNIa} - w_2^{\rm CMB}\right|}{\sqrt{\sigma^2_{w,\rm SNIa} + \sigma^2_{w,\rm CMB}}}, \quad \tau_2 = \frac{\left|\Omega_{\rm M}^{\rm eff,SNIa} - \Omega_{\rm M}^{\rm eff,CMB}\right|}{\sqrt{\sigma^2_{\Omega,\rm SNIa} + \sigma^2_{\Omega,\rm CMB}}}, \tag{91}$$

where the σ_i denote the respective error of the result. Since our distributions are not gaussian, we can get an approximation considering the respective half-length of the respective 68% intervals. This yields $\tau_1 \simeq 0.64\sigma$ and $\tau_2 \simeq 1.12\sigma$, which are small and indicate that both data sets can be combined for a joint analysis.

Lastly, in order to compare the performance of both our TDiff model and wCDM, it will be useful for us to check the DIC coefficient (deviance information criteria), which can be obtained for each model the following way [40]:

$$\mathrm{DIC} = 2\bar{\chi}^2(\mathbf{x}) - \chi^2(\bar{\mathbf{x}}), \tag{92}$$

where $\mathbf{x}$ denotes the respective parameter set of each model and $\bar{x}_i = \int x_i \mathcal{L}^{\rm m}(x_i)\mathrm{d}x_i$ expresses the mean value of the free parameters. Similarly, $\bar{\chi}^2 = \int \chi^2(\mathbf{x})\mathcal{L}(\mathbf{x})\mathrm{d}\mathbf{x}$ indicates the mean value of the χ^2 function. Using (92) yields the following results:

$$\mathrm{DIC}_{\rm TDiff} = 562.05, \ \mathrm{DIC}_{w\rm CDM} = 561.09, \ \mathrm{DIC}_{\Lambda\rm CDM} = 562.81; \tag{93}$$

where, for completion, we also included the analogous ΛCDM SNIa+CMB fit to the ones we performed for the other two models (this fit was equivalent to the wCDM fit but fixing $w = -1$).

Therefore, we can compute

$$\Delta\mathrm{DIC}_1 = \mathrm{DIC}_{\rm TDiff} - \mathrm{DIC}_{w\rm CDM} = 0.96, \tag{94}$$

$$\Delta\mathrm{DIC}_2 = \mathrm{DIC}_{\Lambda\rm CDM} - \mathrm{DIC}_{\rm TDiff} = 0.76; \tag{95}$$

which indicate that there is *weak* evidence in favor of wCDM with respect to our TDiff model, since $0 \leq \Delta\mathrm{DIC}_1 < 2$ according to the standards. Similarly, we obtained $0 \leq \Delta\mathrm{DIC}_2 < 2$, and thus in light of this analysis we see that there is *weak* evidence in favor of the TDiff model with respect to ΛCDM. Consequently, the results obtained in this section indicate that TDiff models provide goodness of fits to CMB and SNIa data statistically similar to those of wCDM and future work regarding these models is thus further motivated. Particularly, the development of the perturbation regime and the full observational analysis including BAO, $H(z)$ data, the power spectrum, etc. look to be of special interest.

Notice how, although the model is compatible with an approximate cosmological constant behavior in the 2-σ region (see Fig. 5), the best fit area lies in the range of w_2 in the interval $(-0.729, -0.677)$. This indicates that, in light of observational data, the TDiff model would favor a non-cosmological constant behavior in the asymptotic future for the dark energy component, with it being phantom in the matter era and there being phantom crossing, as we studied from the single-field dominance regimes.

Fig. 6 summarizes the results of the best fitting SNIa model and its comparison to wCDM, displaying favorable agreement with observations, and also to wCDM, although there start being minor differences between both models at higher redshift values.

[4] https://getdist.readthedocs.io/

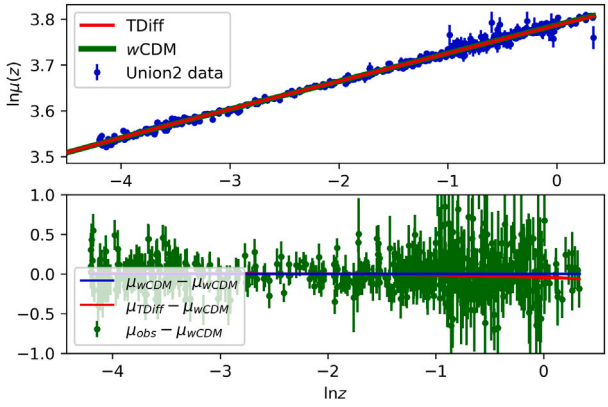

Fig. 6. Best fit (SNIa): comparison to wCDM and observations. Both models exhibit great accordance with observational data from type Ia supernovae and do not differ much from each other. Minor differences start appearing between the models at higher redshift values.

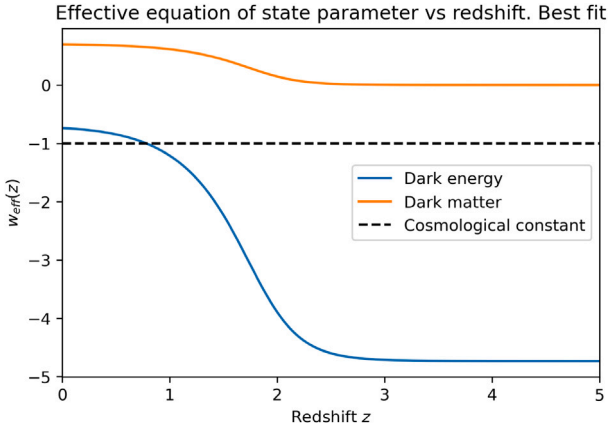

Fig. 7. $w_{\rm eff}(z)$ for the two-parameter best fit. DE behaves as a phantom component under DM domination and its dynamical decay transitions to depict its quintessence w_2 behavior in the future. There is phantom crossing taking place near the current time.

Lastly, we include the evolution of the effective equation of state parameter for the DE and DM components for the best fitting TDiff model in Fig. 7. We see that today DE evolves with an effective equation of state $w_{\rm eff,2}(t_0) \simeq -0.75$. As a result, TDiff models favor the presence of a dynamical DE, starting from phantom at early times and slowly transitioning to usual quintessence DE, with an asymptotic quintessence decay dictated by w_2). Similarly, DM will exhibit a faster decay than that expected from $w_1 = 0$ at recent times as a consequence of the symmetry breaking, without the usual a^{-3} decay being altered during the matter era.

The results obtained throughout this section indicate that this TDiff model should be further explored in the future. Particularly, the Hubble tension problem should be taken into consideration, as other models involving phantom DE have been proven to be favored by observations [9].

It is worth remarking that this time-evolving DE behavior involving phantom-quintessence transitions was obtained without enforcing any type of interaction potential in the Lagrangian, and without the addition of non-canonical or ghost terms in the matter action.

5. Conclusions and future work

In this work, we have considered shift-symmetric theories with two kinetically-driven scalar fields breaking the Diff symmetry down to TDiff and studied their cosmological consequences. We have analyzed

the geometrical condition imposed by the conservation of the total EMT, which still holds as a consequence of the Bianchi identities. When working in a flat FLRW background, this conservation allows us to obtain a geometrical constraint that leads to a particular shape for the lapse function, which cannot be freely chosen now due to the symmetry breaking.

This geometrical constraint enforces an exchange of energy between both fields, as their individual EMTs are not conserved. In light of this fact, we have proposed a dark sector model involving two TDiff scalar fields coupled to gravity through power-law functions of the metric determinant, with one field describing a DM fluid and the other DE. We have regarded the different field domination regimes and showed that, although the equation of state parameters of both fluids are constant, both components will exhibit a different dynamical decay as that corresponding to Diff models with the same constant parameters. Particularly, when imposing that DM decays as a^{-3} at early times, we show that the DE component will present phantom behavior during the matter era for it to slowly transition into quintessential behavior in the future, even if its equation of state parameter takes a constant value larger than minus one. It should be emphasized that this interaction of the dark sector is obtained without including interacting potentials. Moreover, non-canonical kinetic terms have not been considered to obtain phantom behavior. In this framework one naturally obtains an interacting dark sector with a dark energy component that crosses the phantom regime. In addition, the shift symmetry of the fields allows us to describe a dynamical interacting dark sector avoiding fine-tuning problems depending on the specific choice for the potential.

We have also studied the evolution of the energy exchange between the fluids and shown how in these models it is always DE which gains energy from DM. On the other hand, we have also considered a particular analytical model to understand the physics involved in this TDiff dark sector framework. For that model, we have analyzed the form of the interaction kernel, and investigated the decay of the fluids, parameterized through $w_{\mathrm{eff},i}(z)$.

Beyond the simplest dark sector model, we have studied this interacting dark matter-dark energy framework in deeper detail using numerical techniques. We have considered its parameters: w_2 (the equation of state parameter for the DE field, linked to the exponent of the coupling function) and $\Omega_{\mathrm{M}}^{\mathrm{eff}}$ (an effective density parameter at high redshift values, which plays a similar role to the Ω_{M} parameter in ΛCDM). Moreover, we have used the Union2 data for Ia supernovae and fitted our two parameters to these observations to get a first glance regarding the viability of these theories. Our results show compatibility with those data and a goodness of the fit similar to that of wCDM. We also studied the statistical performance and checked that, based on our analyses, there is weak evidence that favors wCDM with respect to our TDiff model, and there is also weak evidence that favors our TDiff model with respect to ΛCDM. It is worth mentioning that these results have been obtained considering two parameters (w_2 and $\Omega_{\mathrm{M}}^{\mathrm{eff}}$), but further and more complete results should be obtained in future work when extending to the full observational analysis using more data sets and more parameters (namely the Hubble constant and the baryonic abundance, as well as the absolute magnitude). That is, after having introduced this shift-symmetric multi-field TDiff model for the first time in this work and studied it from a more theoretical point of view, these first positive results definitely indicate that the model deserves further analyses.

Finally, it is worthy to emphasize that the present work has started a new line of research based on studying multi-field TDiff theories, as we established the theoretical basis for these models and analyzed the interactions arising from the Diff symmetry breaking from a theoretical point of view. We also performed a preliminary observational analysis at the background level that motivates further study of these theories. Consequently, future projects include to investigate the stability under cosmological perturbations of these theories, in order to study structure formation from the TDiff perturbation formalism perspective; the covariantized approach, studied in detail in Ref. [24], could be of special relevance for this purpose. Moreover, one could also analyze the models resulting from considering more general coupling functions or non-homogeneous fields, as well as going beyond the shift-symmetric case and/or breaking the Diff symmetry also in the Einstein–Hilbert action. From an observational point of view, future work will also be done regarding a deeper likelihood analysis using additional data sets, such as (Pantheon+ SH0Es [35,36], the full CMB likelihood, BAO and $H(z)$ [41–44]) and an extended parameter space, together with the possible impact on the Hubble tension problem.

CRediT authorship contribution statement

Diego Tessainer: Writing – review & editing, Writing – original draft, Visualization, Validation, Software, Project administration, Methodology, Investigation, Conceptualization. **Antonio L. Maroto:** Writing – review & editing, Writing – original draft, Validation, Supervision, Resources, Methodology, Investigation, Funding acquisition, Conceptualization. **Prado Martín-Moruno:** Writing – review & editing, Writing – original draft, Validation, Supervision, Resources, Methodology, Investigation, Funding acquisition, Conceptualization.

Declaration of Generative AI and AI-assisted technologies in the writing process

The authors declare that no generative AI or AI-assisted technologies have been used in the writing of the paper.

Declaration of competing interest

The authors declare that they have no known competing financial interests or personal relationships that could have appeared to influence the work reported in this paper.

Acknowledgments

The authors would like to thank Darío Jaramillo Garrido and Alfredo Delgado Miravet for useful comments and discussions regarding TDiff theories. DTB also acknowledges financial help from the Ayudas de Máster IPARCOS-UCM/2023. This work has been supported by the MICIN (Spain) Project No. PID2022-138263NB-I00 funded by MICIU/AEI/10.13039/501100011033 and by ERDF/EU.

Data availability

The external data we used are openly accessible.

References

[1] A.G. Riess, et al., Supernova Search Team Collaboration Collaboration, Observational evidence from supernovae for an accelerating universe and a cosmological constant, Astron. J. 116 (1998) 1009–1038, http://dx.doi.org/10.1086/300499, arXiv:astro-ph/9805201.

[2] S. Tsujikawa, Quintessence: A review, Classical Quantum Gravity 30 (2013) 214003, http://dx.doi.org/10.1088/0264-9381/30/21/214003, arXiv:1304.1961.

[3] C. Armendariz-Picon, V.F. Mukhanov, P.J. Steinhardt, Essentials of k essence, Phys. Rev. D 63 (2001) 103510, http://dx.doi.org/10.1103/PhysRevD.63.103510, arXiv:astro-ph/0006373.

[4] K. Freese, Review of observational evidence for dark matter in the universe and in upcoming searches for dark stars, EAS Publ. Ser. 36 (2009) 113–126, http://dx.doi.org/10.1051/eas/0936016, arXiv:0812.4005.

[5] A.G. Riess, S. Casertano, W. Yuan, L.M. Macri, D. Scolnic, Large magellanic cloud cepheid standards provide a 1% foundation for the determination of the hubble constant and stronger evidence for physics beyond ΛCDM, Astrophys. J. 876 (1) (2019) 85, http://dx.doi.org/10.3847/1538-4357/ab1422, arXiv:1903.07603.

[6] E. Di Valentino, L. Anchordoqui, O. Akarsu, Y. Ali-Haïmoud, L. Amendola, N. Arendse, M. Asgari, M. Ballardini, E. Battistelli, M. Benetti, S. Birrer, F. Bouchet, M. Bruni, E. Calabrese, D. Camarena, S. Capozziello, A. Chen, J. Chluba, A. Chudaykin, W. Yang, Cosmology intertwined II: The hubble constant tension, 2020, http://dx.doi.org/10.48550/arXiv.2008.11284.

[7] E. Abdalla, et al., Cosmology intertwined: A review of the particle physics, astrophysics, and cosmology associated with the cosmological tensions and anomalies, JHEAp 34 (2022) 49–211, http://dx.doi.org/10.1016/j.jheap.2022.04.002, arXiv:2203.06142.

[8] E. Di Valentino, A. Melchiorri, O. Mena, Can interacting dark energy solve the H_0 tension? Phys. Rev. D 96 (4) (2017) 043503, http://dx.doi.org/10.1103/PhysRevD.96.043503, arXiv:1704.08342.

[9] E. Di Valentino, A. Mukherjee, A.A. Sen, Dark energy with phantom crossing and the H_0 tension, Entropy 23 (4) (2021) 404, http://dx.doi.org/10.3390/e23040404, arXiv:2005.12587.

[10] L. Heisenberg, H. Villarrubia-Rojo, J. Zosso, Simultaneously solving the H0 and σ8 tensions with late dark energy, Phys. Dark Univ. 39 (2023) 101163, http://dx.doi.org/10.1016/j.dark.2022.101163, arXiv:2201.11623.

[11] Y. Akrami, et al., CANTATA Collaboration Collaboration, Modified Gravity and Cosmology: An Update by the CANTATA Network, 2021.

[12] T. Clifton, P.G. Ferreira, A. Padilla, C. Skordis, Modified gravity and cosmology, Phys. Rep. 513 (2012) 1–189, http://dx.doi.org/10.1016/j.physrep.2012.01.001, arXiv:1106.2476.

[13] A. Einstein, English translation in the principle of relativity, Siz. Preuss. Acad. Scis. (1919).

[14] W.G. Unruh, Unimodular theory of canonical quantum gravity, Phys. Rev. D 40 (1989) 1048–1052, http://dx.doi.org/10.1103/PhysRevD.40.1048, URL https://link.aps.org/doi/10.1103/PhysRevD.40.1048.

[15] R. Carballo-Rubio, L.J. Garay, G. García-Moreno, Unimodular gravity vs general relativity: a status report, Classical Quantum Gravity 39 (24) (2022) 243001, http://dx.doi.org/10.1088/1361-6382/aca386, arXiv:2207.08499.

[16] G. Ellis, H. van Elst, J. Murugan, J.-P. Uzan, On the trace-free Einstein equations as a viable alternative to general relativity, Classical Quantum Gravity 28 (2011) 225007, http://dx.doi.org/10.1088/0264-9381/28/22/225007.

[17] E. Alvarez, D. Blas, J. Garriga, E. Verdaguer, Transverse Fierz-Pauli symmetry, Nuclear Phys. B 756 (2006) 148–170, http://dx.doi.org/10.1016/j.nuclphysb.2006.08.003, arXiv:hep-th/0606019.

[18] Y.F. Pirogov, Unimodular bimode gravity and the coherent scalar-graviton field as galaxy dark matter, Eur. Phys. J. C 72 (2012) 2017, http://dx.doi.org/10.1140/epjc/s10052-012-2017-y, arXiv:1111.1437.

[19] A.G. Bello-Morales, A.L. Maroto, Cosmology in gravity models with broken diffeomorphisms, Phys. Rev. D 109 (4) (2024) 043506, http://dx.doi.org/10.1103/PhysRevD.109.043506, arXiv:2308.00635.

[20] A.G. Bello-Morales, J. Beltrán Jiménez, A. Jiménez Cano, A.L. Maroto, T.S. Koivisto, A class of ghost-free theories in symmetric teleparallel geometry, 2024, arXiv:2406.19355.

[21] A.L. Maroto, TDiff invariant field theories for cosmology, J. Cosmol. Astropart. Phys. 04 (2024) 037, http://dx.doi.org/10.1088/1475-7516/2024/04/037, arXiv:2301.05713.

[22] D. Jaramillo-Garrido, A.L. Maroto, P. Martín-Moruno, Tdiff in the dark: gravity with a scalar field invariant under transverse diffeomorphisms, JHEP 03 (2024) 084, http://dx.doi.org/10.1007/JHEP03(2024)084, arXiv:2307.14861.

[23] D. Alonso-López, J. de Cruz Pérez, A.L. Maroto, Unified transverse diffeomorphism invariant field theory for the dark sector, Phys. Rev. D 109 (2) (2024) 023537, http://dx.doi.org/10.1103/PhysRevD.109.023537, arXiv:2311.16836.

[24] D. Jaramillo-Garrido, A.L. Maroto, P. Martín-Moruno, Symmetry restoration for TDiff scalar fields, arXiv:2402.17422.

[25] A.L. Maroto, A.D. Miravet, Transverse-diffeomorphism invariant gauge fields in cosmology, Phys. Rev. D 109 (10) (2024) 103504, http://dx.doi.org/10.1103/PhysRevD.109.103504, arXiv:2402.18368.

[26] A.L. Maroto, A.D. Miravet, TDiff-fuelled cosmic magnetic fields, arXiv:2407.04647.

[27] V.A. Rubakov, The null energy condition and its violation, Phys.-Usp. 57 (2014) 128–142, http://dx.doi.org/10.3367/UFNe.0184.201402b.0137, arXiv:1401.4024.

[28] E. Alvarez, A.F. Faedo, Unimodular cosmology and the weight of energy, Phys. Rev. D 76 (2007) 064013, http://dx.doi.org/10.1103/PhysRevD.76.064013, arXiv:hep-th/0702184.

[29] Y. Gouttenoire, G. Servant, P. Simakachorn, Kination cosmology from scalar fields and gravitational-wave signatures, 2021, arXiv:2111.01150.

[30] S. Dutta, R.J. Scherrer, Big Bang nucleosynthesis with a stiff fluid, Phys. Rev. D 82 (2010) 083501, http://dx.doi.org/10.1103/PhysRevD.82.083501, arXiv:1006.4166.

[31] O. Bertolami, P. Carrilho, J. Paramos, Two-scalar-field model for the interaction of dark energy and dark matter, Phys. Rev. D 86 (2012) 103522, http://dx.doi.org/10.1103/PhysRevD.86.103522, arXiv:1206.2589.

[32] K.J. Ludwick, The viability of phantom dark energy: A review, Modern Phys. Lett. A 32 (28) (2017) 1730025, http://dx.doi.org/10.1142/S0217732317300257, arXiv:1708.06981.

[33] R.L. Workman, et al., Particle Data Group Collaboration Collaboration, Review of particle physics, PTEP 2022 (2022) 083C01, http://dx.doi.org/10.1093/ptep/ptac097.

[34] N. Aghanim, et al., Planck Collaboration Collaboration, Planck 2018 results. VI. Cosmological parameters, Astron. Astrophys. 641 (2020) A6, http://dx.doi.org/10.1051/0004-6361/201833910, arXiv:1807.06209; Astron.Astrophys. 652 (2021) C4, Erratum.

[35] D. Scolnic, et al., The pantheon+ analysis: The full data set and light-curve release, Astrophys. J. 938 (2) (2022) 113, http://dx.doi.org/10.3847/1538-4357/ac8b7a, arXiv:2112.03863.

[36] D. Brout, et al., The pantheon+ analysis: Cosmological constraints, Astrophys. J. 938 (2) (2022) 110, http://dx.doi.org/10.3847/1538-4357/ac8e04, arXiv:2202.04077.

[37] R. Amanullah, et al., Spectra and light curves of six type ia supernovae at 0.511 < z < 1.12 and the Union2 compilation, Astrophys. J. 716 (2010) 712–738, http://dx.doi.org/10.1088/0004-637X/716/1/712, arXiv:1004.1711.

[38] P. Ade, N. Aghanim, M. Arnaud, M. Ashdown, J. Aumont, C. Baccigalupi, R. Barreiro, N. Bartolo, E. Battaner, R. Battye, K. Benabed, A. Benoî t, A. Benoit-Lévy, J. Bernard, M. Bersanelli, P. Bielewicz, A. Bonaldi, L. Bonavera, A. Zonca, Planck 2015 results. xIV. Dark energy and modified gravity, Astron. Astrophys. 594 (2015) http://dx.doi.org/10.48550/arXiv.1502.01590.

[39] W. Hu, N. Sugiyama, Small-scale cosmological perturbations: An analytic approach, Astrophys. J. 471 (1995) 542–570, URL https://api.semanticscholar.org/CorpusID:15122385.

[40] D. Spiegelhalter, N. Best, B. Carlin, A. Linde, Bayesian measures of model complexity and fit (with discussion), Journal of the Royal Statistical Society, Series B 64 (2002) 1–34, http://dx.doi.org/10.1111/1467-9868.02022.

[41] A. Riess, S. Casertano, W. Yuan, J. Bowers, L. Macri, J. Zinn, D. Scolnic, Cosmic distances calibrated to 1 and hubble space telescope photometry of 75 milky way cepheids confirm tension with ΛCDM, Astrophys. J. 908 (2021) L6, http://dx.doi.org/10.3847/2041-8213/abdbaf.

[42] M. Moresco, A. Cimatti, R. Jimenez, L. Pozzetti, G. Zamorani, M. Bolzonella, J. Dunlop, F. Lamareille, M. Mignoli, H. Pearce, P. Rosati, D. Stern, L. Verde, E. Zucca, C. Carollo, T. Contini, J.-P. Kneib, O. Le Fevre, S. Lilly, N. Welikala, Improved constraints on the expansion rate of the universe up to z 1.1 from the spectroscopic evolution of cosmic chronometers, Journal of Cosmology and Astroparticle Physics - JCAP 2012 (2012) http://dx.doi.org/10.1088/1475-7516/2012/08/006.

[43] D. Scolnic, D. Jones, A. Rest, y.-c. Pan, R. Chornock, M. Huber, R. Kessler, G. Narayan, A. Riess, S. Rodney, E. Berger, P. Challis, M. Drout, D. Finkbeiner, R. Lunnan, R. Kirshner, N. Sanders, E. Schlafly, K. Smith, The complete light-curve sample of spectroscopically confirmed type ia supernovae from pan-STARRS1 and cosmological constraints from the combined pantheon sample, Astrophys. J. 859 (2017) http://dx.doi.org/10.3847/1538-4357/aab9bb.

[44] R.-Y. Guo, X. Zhang, Constraining dark energy with hubble parameter measurements: An analysis including future redshift-drift observations, Eur. Phys. J. C 76 (2015) http://dx.doi.org/10.1140/epjc/s10052-016-4016-x.